separations

MDPI

Article

Regeneration of Arsenic- and Barium-Poisoned V_2O_5–WO_3/TiO_2 SCR Catalyst

Peilin Xu [1], Xide Sun [1], Chaoqun Wang [1], Dapeng Sun [1], Jianrui Wu [2], Zhongliang Li [2], Haifeng Zou [2] and Yanhua Song [2,*]

[1] Changchun Jidian Energy Technology Co., Ltd., Changchun 130012, China; 6226552@163.com (P.X.); 18904413519@163.com (X.S.); 18143107731@163.com (C.W.); 18543132410@163.com (D.S.)
[2] College of Chemistry, Jilin University, Changchun 130012, China; wjr23@mails.jlu.edu.cn (J.W.); lizhongliang@jlu.edu.cn (Z.L.); haifengzou0431@sohu.com (H.Z.)
* Correspondence: yhsong@jlu.edu.cn

Abstract

Regeneration of catalysts through arsenic and alkaline rare earth removal can not only solve the environmental problems caused by the stacking of deactivated catalysts and arsenic pollution, but also reduce the economic investment required to produce new catalysts. After analyzing the structure and composition of the spent V_2O_5–WO_3/TiO_2 catalysts obtained from a power factory, their existence, form and content were determined for As and Ba. NaClO was used as both an oxidant and a base source in leaching As. It first oxidizes the highly toxic and adsorbed stable As(III) into the more water-soluble As(V). Meanwhile, the OH^- produced by hydrolysis provides an alkaline environment, promoting the conversion of As^{5+} to soluble AsO_4^{3-} and facilitating the desorption and dissolution of As from the catalyst. Taking into account the removal rate of arsenic and the loss of active ingredients, the optimal process conditions were determined. The $BaSO_4$ was removed using the EDTA complexation method and the optimal conditions were determined. The elution and regeneration process not only removed arsenic but also effectively unblocked the pore structure of the catalyst. The redox capacity of the regenerated catalyst was significantly enhanced, and the number and strength of acid sites and the denitrification performance were also effectively restored.

Keywords: regeneration of SCR catalyst; technology of As and Ba removal; sodium hypochlorite; one-step oxidation and base leaching

Check for updates

Academic Editor: Athanasia K. Tolkou

Received: 14 September 2026
Revised: 30 October 2026
Accepted: 2 November 2026
Published: 4 November 2026

Copyright: © 2026 by the authors. Licensee MDPI, Basel, Switzerland. This article is an open access article distributed under the terms and conditions of the Creative Commons Attribution (CC BY) license.

1. Introduction

Nitrogen oxides (NO) are the main pollutants produced by the combustion of fossil fuels and pose a serious threat to the environment and human health through the formation of acid rain, photochemical smog, and low-level ozone [1–3]. Selective catalytic reduction (SCR) catalysts can selectively and efficiently convert NO to N_2 to reduce NO pollution. V_2O_5–WO_3/TiO_2 is a commonly used SCR catalyst [4]. Among these components, TiO_2 is widely used as a carrier due to its stable chemical properties and abundant surface acidic sites, which can promote the adsorption and activation of NH_3. As an active component, V_2O_5 can directly catalyze the oxidation–reduction reaction between NO and adsorbed NH_3. WO_3 is commonly used as a co-catalyst to inhibit the transformation of TiO_2 from a high-activity anatase phase to a low-activity rutile phase, thereby enhancing the high-temperature stability of the catalyst and extending its service life [5–8]. Furthermore, with

the increasing demand for industrial flue gas denitrification, SCR technology has become the main technology for flue gas treatment in industries such as power and steel due to its efficient NO reduction ability. However, SCR catalysts are prone to losing their activity due to poisoning, abrasive wear, and sintering during long-term operation, resulting in a large amount of spent SCR catalysts. The stacking of spent catalysts not only leads to secondary environmental pollution but also represents a significant waste of resources. Therefore, the regeneration and utilization of deactivated catalysts can not only solve environmental pollution problems and reduce resource waste but also lower the cost of replacing catalysts.

As typical toxic pollutants in industrial flue gas, arsenic and alkaline earth ions are easily deposited in the pore structure and active sites of SCR catalysts through diffusion and permeation, forming stable compounds with active components such as V_2O_5 and WO_3 [9–11]. This not only blocks the pore channels of the carrier and reduces gas diffusion efficiency, but also directly damages the catalytic active centers of the catalyst, ultimately leading to a sharp decline in catalyst denitrification performance and a loss of activity. If these As-containing spent SCR catalysts are disposed of through traditional landfill methods, As can easily enter the ecosystem through rainwater leaching, soil adsorption, and other pathways, causing environmental risks such as heavy metal pollution in soil and deterioration of groundwater quality, seriously threatening the survival of animals and plants and human health. If only simple regeneration treatment is carried out on these poisoned catalysts, it is difficult to achieve directional separation and recovery of As, which not only causes waste of high-quality resources such as titanium-based carriers and rare metals, but also cannot fundamentally eliminate pollution hazards [11].

The reported As elution methods for waste SCR catalysis include acid leaching, electrochemical, biological leaching, and alkaline washing methods. The acid leaching method has a higher efficiency in removing As, but it can easily cause damage to the active components of the SCR catalyst and the microstructure of the carrier. Meanwhile, acidic wastewater containing As leads to secondary pollution [12]. As an emerging means of As removal technology, the electrochemical method can generate reactive oxygen species in situ through electrode reactions, regulating the oxidation–reduction potential or achieving ion electro-migration, thereby leading to selective removal of As. This method is clean and green, but consumes a significant amount of energy, and scaling production is expensive [13]. The biological leaching method offers high selectivity and As removal efficiency and is environmentally friendly. However, the bacterial strains applied have high environmental requirements, low stability, and require specialized bioreactors [14]. The alkaline leaching method has a mild process, high As removal efficiency, and low cost; due to these advantages, it is widely used in industrial production. NaOH, $NH_3 \cdot H_2O$, and NH_4HCO_3 are used as leaching agents to remove As from spent catalysts. Oxidizing agents such as H_2O_2 may also be used to enhance the removal efficiency of As [15–17]. For the regeneration of alkaline earth ion-poisoned SCR catalysts, existing research has focused primarily on the mechanism of calcium (Ca) and magnesium (Mg) ion contamination and the technology required to remove it [18–28]. Although contamination with other alkaline earth elements such as barium (Ba) is rarely reported, Ba contamination was found in the spent V_2O_5-WO_3-TiO_2 SCR catalyst studied in this work. As a result, Ba removal technology was developed.

The arsenic in the deactivated catalyst exists in two main forms: As_2O_3 and As_2O_5. The toxicity of As(III) is 60 times that of As(V), and As_2O_5 is more easily removed by reacting with an alkali [13]. Therefore, oxidizing As(III) to As(V) can significantly improve the efficiency of arsenic removal and reduce the risk of operator poisoning [16]. As a commonly used oxidant, NaClO offers high oxidation efficiency, good water solubility, and sufficient reactivity with catalysts. It can quickly and efficiently oxidize As(III) to As(V), and its oxidizability is mild and controllable, causing no damage to the core structure of

the catalyst. Meanwhile, the hydrolysis of NaClO can produce OH^-, further promoting the dissolution of As(V) [29]. Thus, in this work, a one-step oxidation leaching method with NaClO as both the oxidant and alkali source was developed to study the efficient removal of As ions from waste SCR catalysts. Meanwhile, disodium ethylene diamine tetraacetic acid (EDTA) was used as a chelating agent to remove Ba. The effects of temperature, reagent dosage, elution method, etc., on As and Ba removal efficiency were systematically studied, and the optimal process parameters were determined. Furthermore, the mechanism of catalyst poisoning was studied. After regeneration, the denitrification performance of the catalyst in the low-temperature region was significantly improved. This study provides technology for the recycling and regeneration of As and Ba poisoning in catalysts.

2. Materials and Methods

2.1. Materials

The spent V_2O_5–WO_3/TiO_2 honeycomb catalysts used in this work were obtained from Chifeng Power Plant in China. After blowing, high-pressure water gun washing, drying, crushing, and screening, the waste catalyst was screened for particles with a particle size of less than 200 mesh for the experiment. The sodium hypochlorite solution (13 wt% NaClO, 10% available chlorine) was purchased from Tianjin Huadong Reagent Factory, Tianjin, China. The concentrated sulfuric acid (98%) was purchased from Beijing Chemical Plant, Beijin, China. The JFC-2 (CP) and Tween-80 (CP) were purchased from Nantong Chenrun Chemical Co., Ltd., Nantong, China. The ammonium molybdate (A.R.), ammonium metavanadate (A.R.), disodium ethylenediaminetetraacetate (EDTA, A.R.), and hydrated ammonium metatungstate (A.R.) were purchased from Shanghai Aladdin Biochemical Technology Co., Ltd., Shanghai, China. All reagents were used directly without further purification treatment.

2.2. As and Ba Leaching Experiments

2.2.1. As Leaching Experiments

First, 0.08, 0.23, 0.38, 0.53, or 0.78 mL of the NaClO solution were taken and added to 100 mL of deionized water to obtain NaClO solutions with a NaClO content of 0.01, 0.03, 0.05, 0.07, and 0.1 wt% and available chlorine content of 0.008, 0.023, 0.038, 0.054, and 0.077%, respectively. Secondly, 1.0 g of the catalyst was added to this solution. Then, the mixture was placed in a water bath and reacted for 1 h at fixed temperatures (50, 60, 70, and 80 °C). The influence of the elution method on As removal was also investigated, including three groups of experiments: one was eluted for 1 h, the second was eluted continuously for 2 h, and the third was eluted in two stages for 1 h each. After the elution, the concentration of As leached into the solution was determined by ICP-OES and the removal efficiency was calculated using Equation (1):

$$\eta(\%) = \frac{m_{elution}}{m_{initial}} \times 100\% \quad (1)$$

where η (%) is the removal efficiency of the poison ion, and $m_{initial}$ (g) and $m_{elution}$ (g) are the initial weight of poison ions in the spent catalyst and the weight eluted to the solution. Each experiment was replicated three times.

2.2.2. Ba Leaching Experiment

First, after As removal, 1.0 g of the catalyst was added to 100 mL of deionized water, and then 1 wt% EDTA was added to the solution. The pH of the solution was adjusted to 5–9 using H_2SO_4 or NaOH. The obtained suspension was placed into a water bath and maintained at a fixed temperature (25, 40, 50, and 60 °C) for 1 h. After the elution, the

concentration of Ba leached into the solution was determined by ICP-OES and the removal efficiency was calculated using Equation (1). Each experiment was replicated three times.

2.2.3. Regeneration of Spent Catalyst

First, 1 g of spent catalyst was added to a 100 mL 0.1 wt% NaClO solution, followed by leaching in 0.1 wt% NaClO solution at 70 °C for 1 h to remove As. This As-leaching process was conducted twice under the same conditions. Secondly, the obtained catalyst was separated from the NaClO solution through suction filtration and added to a solution containing 1 wt% EDTA with pH = 8 (adjusted by NaOH) and stirred at 200 r/min for 1h at 50 °C to remove Ba. Thirdly, the treated catalyst was separated and eluted using a mixed solution containing H_2SO_4, 0.1wt% JFC-2 and 0.1 wt% Tween 80 at pH = 3 for 3 h to achieve deep removal of residual impurities in the catalyst pores. Finally, the catalyst after multi-step leaching was separated by suction filtration and mixed with a solution containing 1 wt% NH_4VO_3, 1 wt% $(NH_4)_6H_2W_{12}O_{40}{\cdot}XH_2O$, and 0.5 wt% $(NH_4)_2MoO_4$ and aged for 1 h to ensure uniform adsorption of the active components on the catalyst. The obtained catalyst was dried in a blast drying oven at 120 °C for 2 h and then calcined at 500 °C for 2 h to obtain the regenerated catalyst. The flow chart of the regeneration process is shown in Figure 1.

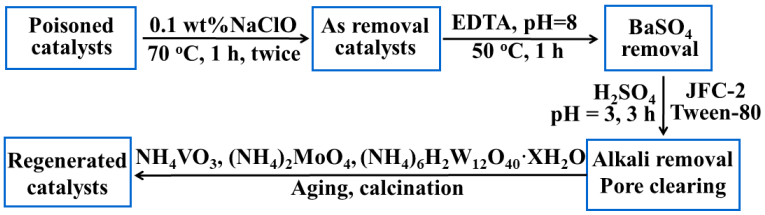


Figure 1. Flow chart of the regeneration process.

2.3. Characterization

The structure of the solid sample was measured using an X-ray diffractometer (XRD, Panaco Empyrean, PANalytical B.V., Almelo, The Netherlands) with the range of $2\theta = 10°{\sim}80°$. The element content of the solid sample was tested using an X-ray fluorescence spectrometer (XRF, ZSX Primus IV, Rigaku Beijing Co., Ltd., Beijing, China). The specific surface area and pore structure of the catalyst were tested using a nitrogen adsorption–desorption analyzer (BET, ASAP 2020 V4.00, Micromeritics Instrument Co., Ltd., Norcross, GA, USA). The elemental composition and chemical valence states of the catalyst surface were characterized using X-ray photoelectron spectroscopy (XPS, ESCALAB 250Xi, Thermo Fisher Scientific Co., Ltd., Waltham, MA, USA). The content of As, Ba, V, and W in the solution was tested using inductively coupled plasma optical emission spectroscopy (ICP-OES, Plasma 1500, NCS Testing Technology Co., Ltd., Beijing, China). The acidic sites and redox performance of the catalyst before and after elution were tested using ammonia gas temperature-programmed desorption (NH_3-TPD) and hydrogen gas temperature-programmed reduction (H_2-TPR) (AutoChem II 2920, Micomerics Instruments, Inc., Norcross, GA, USA) under an activation temperature of 400 °C and a temperature range of 100–900 °C for H_2-TPR; the temperature range for programmed temperature rise desorption is 50–600 °C.

2.4. Denitrification Performance Test

The denitrification performance of the catalyst was carried out on a fixed-bed quartz reactor at atmospheric pressure. The mixed feed gases, with a total flow rate of 200 mL/min, consisted of 500 ppm of NO, 5 vol% O_2, and 500 ppm NH_3. The reaction temperature range was 150–500 °C, and the SCR catalyst was stably equilibrated for 60 min at each 50 °C

increment. The denitrification activity and N_2 selectivity of the SCR catalyst at different temperatures were calculated according to Formulas (2) and (3) [30]:

$$\omega_{NO}(\%) = \frac{C_{NO_{in}} - C_{NO_{out}}}{C_{NO_{in}}} \times 100\% \quad (2)$$

$$S_{N_2}(\%) = 1 - \frac{2C_{N_2O_{out}}}{C_{NO_{in}} - C_{NO_{out}} + C_{NH_{3in}} - C_{NH_{3out}}} \times 100 \quad (3)$$

where $C_{NO_{in}}$ and $C_{NO_{out}}$ represent the concentration of NO at the inlet and outlet, respectively; $C_{N_2O_{out}}$ represents the concentration of N_2O at the outlet; and $C_{NH_{3in}}$ and $C_{NH_{3out}}$ represent the concentration of NH_3 at the inlet and outlet, respectively.

3. Results and Discussions

3.1. Analysis of Catalyst Structure and Element Content

The element contents of the fresh and poisoned catalysts are listed in Table 1. The results showed that there were no As and Ba elements in the fresh catalyst, indicating that the catalyst was poisoned by As and Ba through their use in denitrification in the power factory. The contents of As_2O_3 and BaO in the poisoned catalyst are as high as 2.02% and 2.46%, respectively, which may be the main factors causing catalyst deactivation.

Table 1. Element content of the fresh and poisoned catalyst.

Sample	Content (%)							
	TiO_2	WO_3	V_2O_5	SiO_2	As_2O_3	MoO_3	BaO	SO_3
F	80.87	3.27	0.68	4.11	-	0.07	-	-
P	77.59	3.32	0.63	5.97	2.02	0.06	2.46	3.018

Notes: F and P represent the fresh and poisoned catalysts, respectively.

XRD characterization was performed on the fresh and poisoned catalysts in order to reveal the effect of the poisoning process on the crystal structure of the catalyst; the results are presented in Figure 2. The fresh catalyst was anatase TiO_2 without impurities. After poisoning, the main peaks were consistent with PDF 89-4921($2\theta \approx 25.3°$, 37.8°, 48.0°) [31], indicating that the main phase of the poisoned catalyst was also anatase TiO_2. No diffraction peaks corresponding to V_2O_5, WO_3, or MoO_3 crystals were observed, indicating that the active component maintains a highly dispersed state after poisoning, and no crystal-phase precipitation or aggregation occurs. The results show that the introduction of As and Ba did not change the main structure of the catalyst. Meanwhile, there were some weak peaks located at $2\theta \approx 23.8°$, 28.2°, 32.8°, and 43.0°, as shown in Figure 2b, which correspond to standard data for PDF 76-0214, indicating that the impurity phase is $BaSO_4$ [32]. The appearance of $BaSO_4$ is mainly due to the precipitation reaction between Ba^{2+} ions introduced from coal combustion and the SO_4^{2-} generated by the oxidation of SO_2 in flue gas on the catalyst surface, leading to the deposition of insoluble crystalline $BaSO_4$ on the catalyst surface and pores [33].

To investigate the present state of As in the waste catalyst, XPS characterization was performed. It can be seen from the full XPS spectrum in Figure 3a that the main elemental signals on the surface of the waste catalyst include O 1s, C1s, Ti 2p, V2p, W 4f, Mo 3d, Ba 3d, S 2p and As 3d, directly confirming the adsorption and deposition of As and Ba on the catalyst surface. In addition, as shown in Figure 3b, through peak fitting analysis, there are two forms of As in the spectrum: As(III) (with a binding energy of about 44–45 eV) and As(V) (with a binding energy of about 45–46 eV) [34]. The content ratio of As(V) to As(III)

is calculated to be 60% to 40%. The oxidation of As(III) to As(V) is common in the poisoned catalyst and may be ascribed to two mechanisms: one is induced by surface-adsorbed O_2, and the other is the oxidation–reduction reaction between As(III) and V(V) in V_2O_5, generating As(V) and V(IV). This conversion process also reveals the dynamic surface reaction that occurs during catalyst deactivation [35].

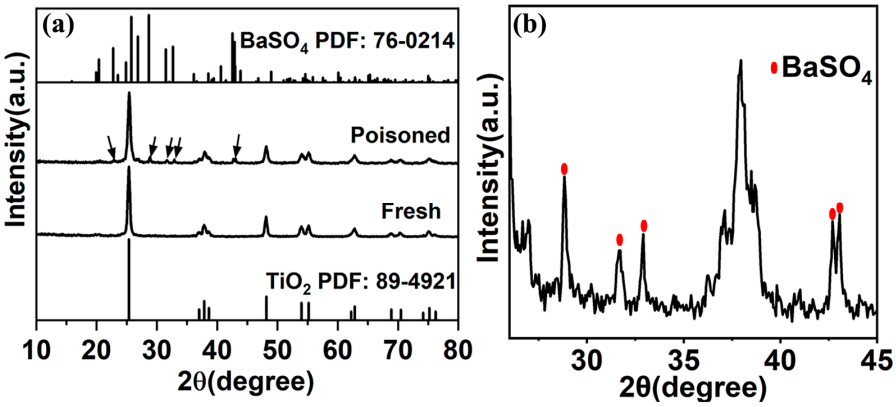


Figure 2. XRD patterns of fresh and poisoned catalysts (**a**) (the peaks indicated by arrows are the diffraction peaks of $BaSO_4$) and enlarged XRD pattern of the poisoned catalyst (**b**).

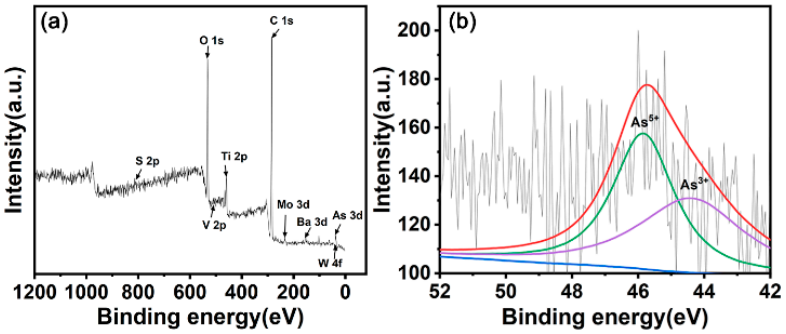


Figure 3. XPS characterization of the poisoned catalyst: (**a**) full XPS survey spectrum; (**b**) high-resolution XPS spectrum of the As element. (Red line: fitting line of total peak; green and purple line: fitting line of peaks of As^{5+} and As^{3+}; blue line: base line).

3.2. Optimization of as Removal Process for Spent Catalyst

3.2.1. The Influence of Temperature on as Removal Efficiency

Figure 4 shows that the elution temperature has a significant impact on the removal of As and the loss of the active component V in the SCR catalyst. With the increase in elution temperature, the removal efficiency of As shows a significant upward trend. When the leaching temperature is 80 °C, the elution efficiency of As in the high-concentration NaClO solution exceeds 80%, indicating that heating can effectively enhance the removal efficiency of As. This result can be attributed to the endothermic hydrolysis characteristics of NaClO, promoting the generation of HClO. The HClO generated by NaClO hydrolysis in aqueous solution has strong oxidizing properties, which can quickly oxidize the highly toxic and adsorption-stable As(III) on the catalyst surface to the more water-soluble As(V), thereby greatly improving the arsenic elution efficiency [29]. However, with the increase in temperature, there is significant loss of active components in the catalyst, including V_2O_5 and WO_3. Both V_2O_5 and WO_3 are typical amphoteric oxides that prefer to react with alkali, generating soluble sodium metavanadate and sodium tungstate, which are lost with the leaching solution [36]. It can be seen from Figure 4b,c that the loss of V is relatively more significant. Under the leaching condition of 80 °C and 0.1 wt% NaClO,

the loss rate of V reaches up to 35%. Although the loss rate of W is relatively low, it also shows a slow upward trend with increasing temperature. Therefore, the enhancement of leaching temperature has a dual effect: the removal efficiency of the target impurity As can be enhanced, but the loss of active components can also be increased. Taking into account the removal efficiency of As and the loss rates of V and W, the elution temperature is determined to be 70 °C.

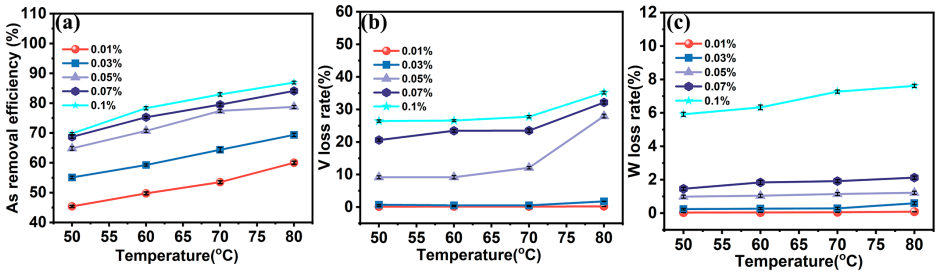


Figure 4. As removal efficiency (**a**) and loss rates of vanadium (**b**) and tungsten (**c**) under different temperatures. Error bars represent standard deviations of triplicate experiments.

3.2.2. The Effect of NaClO Concentration on as Removal Efficiency

Figure 5a shows trends of As removal efficiency with NaClO concentration. The elution efficiency of As shows a significant upward trend with an increase in the NaClO concentration, which is closely related to the As poisoning mechanism of the SCR catalyst and the chemical properties of NaClO. The core essence of As poisoning in SCR catalysts is that gaseous As_2O_3 in the flue gas diffuses into the micropores of the catalyst and forms stable As-O-Ti/V coordination bonds with active sites such as the V^{5+}-OH and Ti^{4+}-OH acidic sites of the V_2O_5–WO_3/TiO_2 catalyst through specific adsorption. This strong chemical bond not only directly occupies the catalytic active center, but also blocks the catalyst pores, leading to a decrease in its denitrification performance [16,37]. The strong oxidizing property of NaClO provides a key solution for the removal of As. The HClO and OH^- generated by its hydrolysis in aqueous solution have dual effects on oxidation and dissociation [29]. They can directly destroy the stability of As-O-Ti/V coordination bonds, weaken the binding force between As and the catalyst surface, and rapidly oxidize insoluble As(III) to more water-soluble As(V), ultimately causing As(V) to completely dissociate from the catalyst surface and be removed with the eluent. Therefore, increasing the concentration of NaClO can further enhance this synergistic effect and promote the continuous improvement in elution efficiency. Further analysis reveals that an increase in NaClO concentration also leads to a synchronous increase in V and W loss rates. Based on the comprehensive consideration of elution efficiency and retention of active components, the optimal concentration of NaClO in the elution treatment of the catalyst is 0.1 wt%.

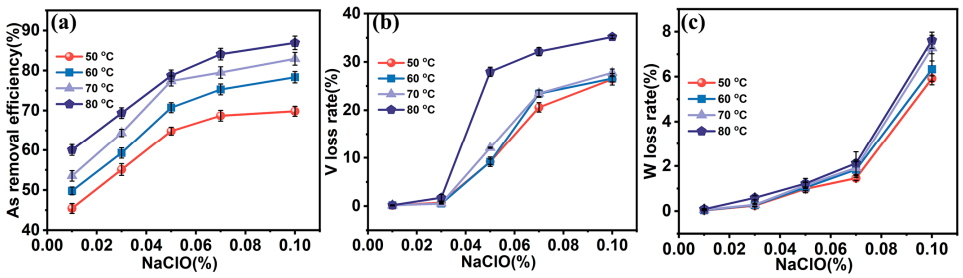


Figure 5. Arsenic removal efficiency (**a**) and loss rates of vanadium (**b**) and tungsten (**c**) under different NaClO concentrations. Error bars represent standard deviations of triplicate experiments.

3.2.3. The Influence of Elution Mode on as Removal Efficiency

Three elution modes, leaching for 1 h, 2 h, and twice for 1 h each time, were chosen to investigate the effect on the As removal efficiency. The results are shown in Figure 6. It can be seen that as the concentration of NaClO increases from 0.01 wt% to 0.1%, the As removal efficiency of all three elution modes shows a gradual increase. The treatment method of single elution for 1 h resulted in a relatively gradual improvement in As removal efficiency, increasing from 53% to 72%. When extending the elution time to 2 h, the As removal efficiency increased to 83%. When using a two-step elution strategy of 1 h for each step, the As removal efficiency remained the highest among the three modes, increasing from the initial 69% to over 87%, which reflects the promoting effect of two-step elution on As removal. This difference is mainly due to the fact that two-step elution can avoid efficiency reduction caused by target ion enrichment in continuous elution by replacing the fresh elution solution. Meanwhile, the effect of leaching time on the loss rates of vanadium and tungsten is presented in Figure 6b,c. The loss rates of V and W show a slight increase as the leaching time is prolonged.

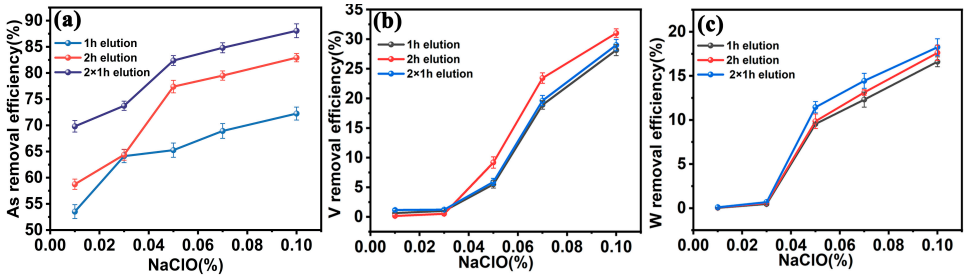


Figure 6. Effect of elution time on As (**a**) removal and V (**b**) and W (**c**) loss rates. Error bars represent standard deviations of triplicate experiments.

3.3. Optimization of $BaSO_4$ Removal Process for Spent Catalyst

EDTA is a well-known and commonly used complexing agent that interacts with many cations and inhibits their precipitation [38]. In this work, the EDTA solution was used as the leaching agent to remove $BaSO_4$ from the poisoned V_2O_5–WO_3/TiO_2 catalyst. The effect of leaching conditions, including pH, temperature, time, and EDTA content, on the $BaSO_4$ removal efficiency was investigated, and the results are shown in Figure 7. Figure 7a illustrates that pH has a significant effect on the removal efficiency of $BaSO_4$. When the pH is lower than seven, the removal efficiency is below 35%. When the pH is eight, the removal efficiency is higher than 97%. When the pH is nine, the removal efficiency shows a small decrease. Therefore, the optimal pH for $BaSO_4$ removal is eight. This result may be ascribed to the protonation state of EDTA and stability of the Ba-EDTA complex depending on the pH. In aqueous solution, EDTA exists as a compound of H_4Y at low pH and dissociates increasing numbers of protons to form species of H_3Y^-, H_2Y^{2-}, HY^{3-} or Y^{4-} as the pH increases. Stable chelates are formed with the $Y_4{}^-$ species, and the stability of these chelates affects the equilibrium between the variously deprotonated species of EDTA [39,40]. The conditional formation constants of Ba-EDTA at pH = 5, 6, 7, 8, and 9 are 1.41, 3.21, 4.54, 5.59, and 6.58, respectively [41]. This means that the stability of the Ba-EDTA complex increases with increasing pH. Therefore, the removal efficiency increases with pH. However, as the pH value increases, the probability of vanadium and tungsten being dissolved in the form of anions increases, and these anions may form precipitates with barium ions and deposit on the catalyst, reducing the removal efficiency of $BaSO_4$. As shown in Figure 7b, the removal efficiency of $BaSO_4$ becomes higher with the increase in temperature. Although $BaSO_4$ is insoluble, it dissociates in solution: $BaSO_4 \rightleftharpoons Ba^{2+} + SO_4{}^{2-}$. As the temperature increases, the dissociation constant increases [42], promoting the generation of Ba^{2+} ions

and Ba-EDTA compounds, thereby facilitating $BaSO_4$ removal. From Figure 7c,d, it can be seen that the optimal leaching time is 1 h, the optimal content of EDTA is 1 wt% and the removal efficiency of $BaSO_4$ can reach nearly 100%.

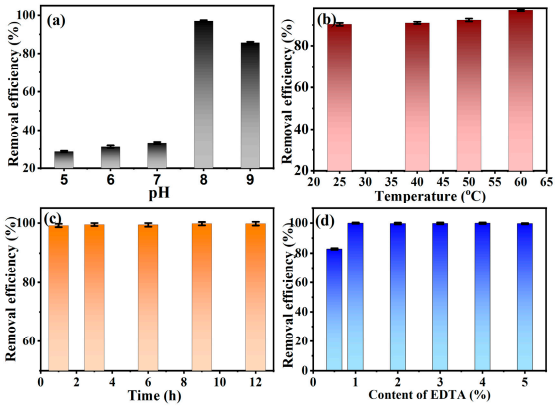


Figure 7. $BaSO_4$ removal efficiency under different conditions: (**a**) pH; (**b**) temperature; (**c**) leaching time; (**d**) content of EDTA. Error bars represent standard deviations of triplicate experiments.

3.4. Characterization and Redox Performance Analysis of Regenerated Catalysts

The As poisoning of vanadium-based catalysts mainly originates from the oxidation of gaseous As_2O_3 to As_2O_5 on the catalyst surface, forming a dense coating that blocks the active sites and pores, destroys the V^{5+}-O-V^{5+} active center structure, and inhibits the $V^{5+} \rightarrow V^{4+}$ redox cycle. The effects of As on the structural changes in active centers, redox ability, acidic sites, and pore structure were investigated using characterization methods such as XRD, XRF, BET, H_2-TPR, and NH_3-TPD.

3.4.1. XRD Analysis of the Regenerated Catalyst

The XRD patterns of the poisoned and regenerated catalysts are shown in Figure 8. The main structure of the regenerated catalysts does not change, maintaining the anatase phase of TiO_2. Compared with the poisoned catalyst, the peaks corresponding to $BaSO_4$ disappear, confirming the successful removal of $BaSO_4$ crystals deposited on the catalyst.

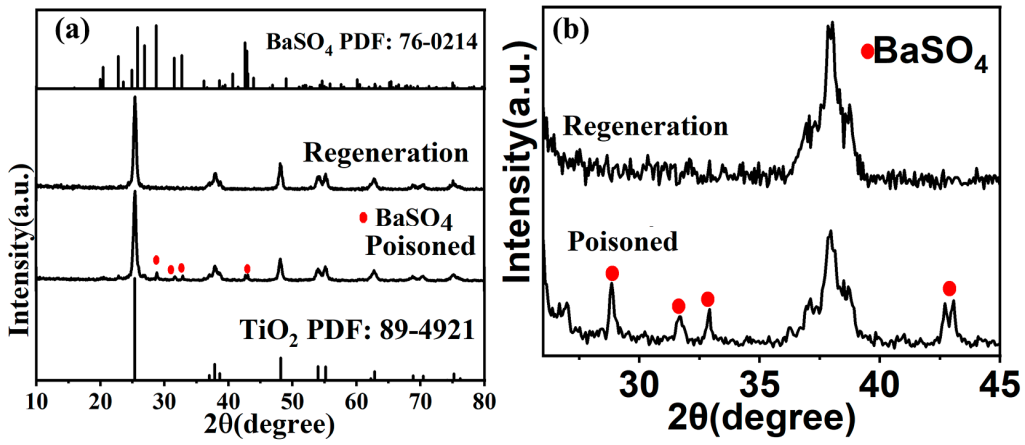


Figure 8. XRD patterns of poisoned and regenerated catalysts and the standard patterns of TiO_2 and $BaSO_4$ (**a**); the enlarged patterns of poisoned and regenerated catalysts (**b**).

3.4.2. Component Analysis of the Regenerated Catalyst

Table 2 lists the contents of the main components of the poisoned, leached, and regenerated catalysts. With leaching via NaClO and the EDTA solution, the As and Ba were

removed effectively. Meanwhile, the content of active components such as V_2O_5, WO_3, and MoO_3 decreased slightly. After regeneration, the active components were effectively supplemented. These results confirm that this leaching and regeneration technology not only achieves the deep removal of impurities and precise control of active components, but can also optimize the chemical composition of the catalyst.

Table 2. Contents of the components of poisoned, leached, and regenerated catalysts.

Component	Poisoned Catalyst (%)	Leached Catalyst (%)	Regenerated Catalyst (%)
TiO_2	77.59	84.74	82.99
WO_3	3.32	2.90	3.27
V_2O_5	0.63	0.34	1.26
SiO_2	5.97	5.50	5.68
As_2O_3	2.02	0.27	0.21
MoO_3	0.06	0.01	0.33
BaO	2.46	-	-

3.4.3. BET Analysis

Figure 9a,b show the N_2 adsorption–desorption curves of the poisoned and regenerated catalysts. Both the curves exhibit a typical IV isotherm with a hysteresis loop, characteristic of mesoporous materials. Compared with the poisoned sample, the regenerated sample showed a higher adsorption capacity under the same relative pressure, indicating that the elution process effectively removed impurities from the catalyst pores, resulting in an increase in specific surface area and pore volume. The surface areas for the poisoned and regenerated catalysts are 40.37 m^2 g^{-1} and 51.99 m^2 g^{-1}, respectively. The inset pore size distribution curve shows that the average pore sizes are 23.49 nm and 21.54 nm for the poisoned and regenerated catalysts, confirming that this elution treatment can effectively remove blockages and impurities in the catalyst pores, significantly increasing their specific surface area. The slight decrease in average pore size indicates an increase in the proportion of small-size mesopores. The optimization of the pore structure mentioned above can not only provide more active sites for the reaction but also accelerate the mass transfer efficiency between reactants and products, which is conducive to the improvement in catalytic performance.

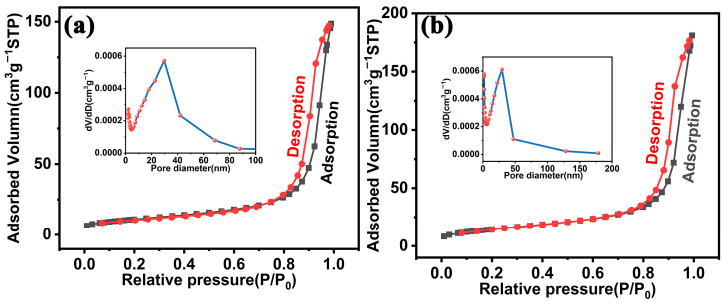


Figure 9. N_2 adsorption–desorption curves of poisoned (**a**) and regenerated (**b**) catalysts (insets are the pore distribution curves).

3.4.4. SEM Analysis

SEM measurements were performed on fresh, poisoned and regenerated catalysts and the results are shown in Figure 10. It can be seen that the morphology of all catalysts was nanoparticles with a diameter of about 50 nm. The results demonstrated that the regeneration process has little effect on the morphology of the catalyst.

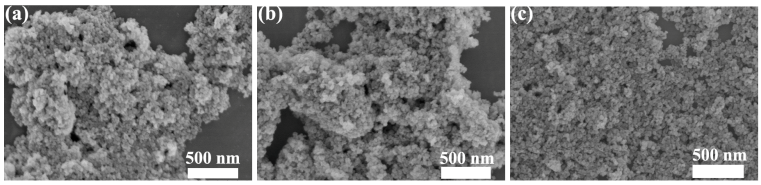


Figure 10. SEM images of the fresh (**a**), poisoned (**b**), and regenerated (**c**) catalysts.

3.4.5. Analysis of Catalyst Redox Performance

H_2-TPR is a traditional method for characterizing the redox performance of catalysts, which can intuitively reflect the reduction difficulty, quantity, and surface chemical environment of active species by detecting hydrogen consumption peaks at different temperatures. The lower the temperature corresponding to the reduction peak, the stronger the oxidation–reduction ability of the sample [43]. For V_2O_5-based SCR catalysts, their essential catalytic process relies entirely on the reversible oxidation–reduction cycle of $V^{5+} \rightarrow V^{4+}$ active sites. In the reaction, V^{5+} acts as an active site to activate NH_3 and is reduced to V^{4+}. Subsequently, V^{4+} is oxidized by O_2 in the flue gas to V^{5+}, completing the cycle to maintain sustained catalytic activity. Therefore, the redox ability of the catalyst directly determines the efficiency of this cycle [44]. According to the composition analysis results, the content of V_2O_5 and MoO_3 after regeneration is higher than that of the poisoned catalyst. In order to eliminate the redox changes caused by the increase in V_2O_5 content, the H_2-TPR data was normalized to the vanadium content. Figure 11 shows the H_2-TPR spectra of the fresh, poisoned, and regenerated catalysts. For the fresh catalyst, the reduction peaks located at 487 °C and 456 °C correspond to the reduction process of the active species $W^{6+} \rightarrow W^{4+}$ and $V^{5+} \rightarrow V^{3+}$ in the V_2O_5-based SCR catalyst [45,46], respectively, and the high-temperature peak at 762 °C is assigned to the reduction of W^{4+} to W^0 [30]. For the poisoned sample, the wide reduction peak of $V^{5+} \rightarrow V^{3+}$ is shifted to 407 °C, which is associated with the overlap of $V^{5+} \rightarrow V^{3+}$, $W^{6+} \rightarrow W^{4+}$, and $As^{5+} \rightarrow As^0$ [47]. The lower-temperature reduction peak of the poisoned catalyst indicated that arsenic contributed to promoting the reducibility of the V_2O_5–WO_3/TiO_2 catalyst, which may enhance the formation probability of N_2O and then reduce the N_2 selectivity [46]. After regeneration, the low-temperature peak shifted to a higher temperature and the peak was weaker than that of the poisoned catalyst, which resulted in a slight decrease in catalytic activity and enhancement of N_2 selectivity.

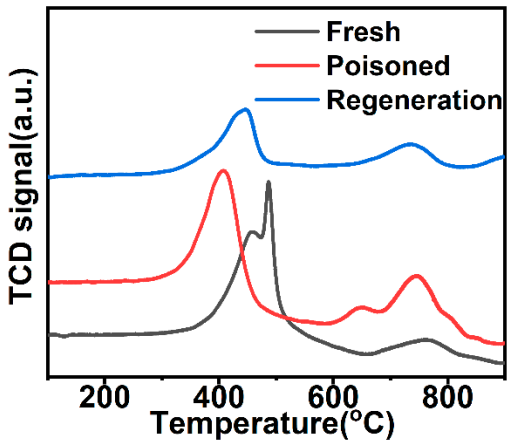


Figure 11. H_2-TPR curves of the catalysts before and after regeneration.

3.4.6. Analysis of Catalyst Surface Acidity

The main denitrification reaction of the V_2O_5–WO_3/TiO_2-based SCR catalyst is the selective catalytic reduction of NO_x by NH_3, which starts with the key step of selective

adsorption and activation of NH_3. The acidic sites on the catalyst surface are the exclusive adsorption and activation sites of NH_3, and their quantity, intensity, and distribution directly determine the adsorption amount and activation efficiency of NH_3, thereby dominating the overall rate and efficiency of the denitrification reaction [48]. The deactivation process caused by As poisoning can significantly damage the surface acidic sites of catalysts, resulting in a decrease in their quantity and strength. Therefore, targeted characterization of surface acidic sites was conducted in order to clarify their changes after catalyst deactivation and regeneration. In order to eliminate the surface acidic site changes caused by the increase in V_2O_5 content, the NH_3-TPD data was normalized to the vanadium content. Figure 12 shows the NH_3-TPD spectra of the fresh, poisoned, and regenerated catalysts, which intuitively reflect the acidity and strength of the acid sites on the catalyst surface. As shown in the figure, all catalysts exhibit a broad peak composed of three distinct NH_3 desorption peaks. Among them, the desorption peak at around 150 °C in the low-temperature region can be attributed to the physical adsorption of NH_3 and the desorption process of NH_4^+ formed by protonation on weak Brønsted acid sites [49]. The broadening desorption peaks in the high-temperature range of 200–450 °C correspond to the characteristic signal of mid-strong and strong acid sites on the catalyst, mainly derived from the desorption of NH_3 by chemical adsorption on Brønsted and Lewis acid sites [50]. Compared with the poisoned catalyst, the two NH_3 desorption peaks of the regenerated catalyst are sharper, and the peak area is significantly increased, indicating that the regeneration process effectively repairs the acidic structure of the catalyst. The method not only restored the acid sites, but also preserved sufficient intermediate and strong acid sites. The dispersion of acid sites was optimized and the aggregation or deactivation of acid sites caused by poisoning was reduced. Abundant and well-dispersed acid sites can provide sufficient adsorption and active centers for the SCR reaction, promoting efficient activation of NH_3 and selective reduction of NO_x, reflecting the remediation effect of this regeneration process on the acid sites of poisoned catalysts.

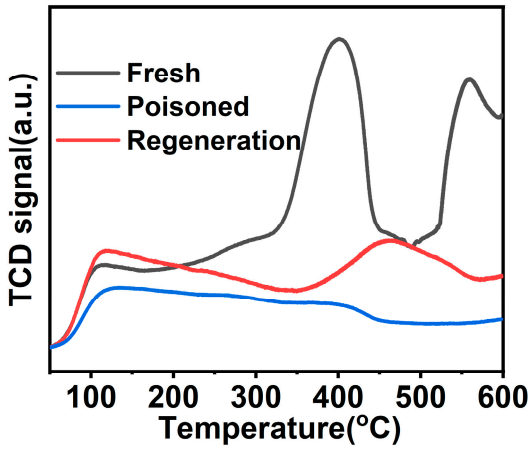


Figure 12. NH_3-TPD curves of the catalyst before and after regeneration.

3.4.7. Denitrification Performance

NO conversion activity and N_2 selectivity were evaluated to determine the denitrification performance of the regenerated catalyst. The results are shown in Figure 13. Regeneration treatment can significantly restore the NO conversion activity of the poisoned catalyst. As shown in Figure 13a, within the same temperature range, the low-temperature activity of the poisoned sample is severely lowered, with NO conversion rates of only 10–70% at 150–250 °C. After regeneration, the catalyst can achieve 100% NO removal at 250 °C, with a much higher activity level than the poisoned catalyst and a slightly lower

activity than that of the fresh catalyst. Although the poisoned catalyst exhibited similar NO conversion efficiency to the fresh catalyst at the temperature range of 300 to 450 °C, its N_2 selectivity of the poisoned catalyst was lower, as shown in Figure 13b. The reason for this may be that a part of NH_3 was adsorbed and activated during the SCR reactions and reacted with NO + O_2 to produce N_2O [46]. After regeneration, both NO conversion and N_2 selectivity were restored, so they were similar to those of the fresh catalyst. This result fully demonstrates that regeneration treatment can effectively remove toxic species and restore catalytic activity for deactivated denitrification catalysts, making them promising for industrial application and providing important experimental support for the resource utilization of industrial waste catalysts.

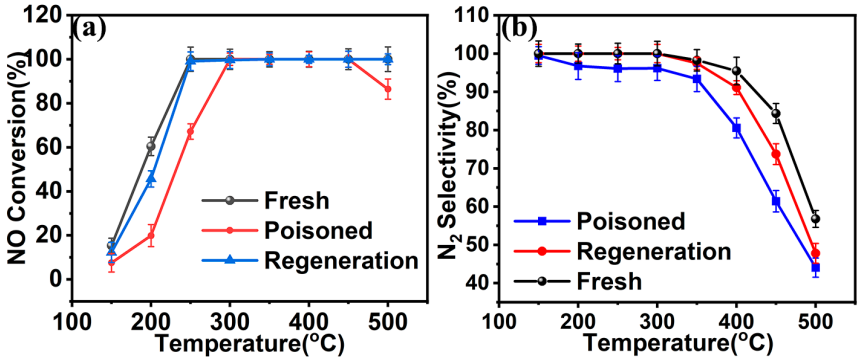


Figure 13. NO conversion (**a**) and N_2 selectivity (**b**) performance of fresh, poisoned, and regenerated catalysts.

4. Conclusions

Based on the analysis of the structure and elements of the poisoned catalyst, NaClO and EDTA solutions can be used to remove As and $BaSO_4$ impurities. HClO generated by the hydrolysis of NaClO can be used to oxidize the highly toxic and adsorption-stable As(III) to the more water-soluble As(V), thereby breaking the As-O-Ti/V coordination bond. At the same time, the OH^- generated by hydrolysis of NaClO provides an alkaline environment, promoting the conversion of As(V) to soluble AsO_4^{3-} and facilitating the desorption and dissolution of As from the catalyst. The optimal process conditions were determined. After As and Ba removal and regeneration, the oxidation–reduction ability of the catalyst is significantly enhanced, and the number and strength of acidic sites are effectively repaired. The denitrification performance is effectively restored, indicating that this regeneration process can effectively achieve the regeneration and utilization of deactivated denitrification catalysts.

Author Contributions: Conceptualization, Y.S. and X.S.; methodology, X.S. and Y.S.; software, C.W.; validation, D.S. and Z.L.; formal analysis, P.X. and J.W.; investigation, P.X. and J.W.; resources, X.S.; data curation, J.W.; writing—original draft preparation, P.X.; writing—review and editing, J.W.; visualization, C.W. and Z.L.; supervision, Y.S. and H.Z.; project administration, X.S. All authors have read and agreed to the published version of the manuscript.

Funding: This research received no external funding.

Data Availability Statement: The original contributions presented in this study are included in the article. Further inquiries can be directed to the corresponding author.

Conflicts of Interest: Authors P.X., X.S., C.W., and D.S. were employed by the company Changchun Jidian Energy Technology Co., Ltd. The remaining authors declare that the research was conducted in the absence of any commercial or financial relationships that could be construed as potential conflicts of interest.

References

1. Zeng, P.; Zhou, Z.; Liu, L.; Yu, X.; Liu, X.; Xu, M. Wide-temperature NO_x removal enabled by synergistic atomically dispersed Ce-V dual sites: Activation of the rate-determining step. *J. Colloid. Interf. Sci.* **2026**, *702*, 138888. [CrossRef] [PubMed]
2. Zhou, Q.; Zhu, B.; Wang, Y.; Zhang, Z.; Mao, X.; Tao, M.; Zhang, H.; Tang, C. Breaking the activity-selectivity trade-off by physically mixing MnO_x-CeO_2 catalysts with HZSM-5 for NO selective catalytic reduction. *Appl. Catal. B Environ. Energy* **2026**, *381*, 125881. [CrossRef]
3. Hong, H.J.; Yoo, H.; Jeon, J.H.; Kim, H.S.; Lee, J.Y. Differential adsorption of vanadium(V) and tungsten(W) on ion exchange resins: A novel approach for separation and recovery of spent catalyst leachate. *J. Clean. Prod.* **2023**, *426*, 139157. [CrossRef]
4. Li, Y.Y.; Zhang, T.R.; Niu, X.Y.; Zhu, Y.J. Vanadium-based catalysts for selective catalytic reduction of NO_x with ammonia: Synthesis, poisoning mechanism, regeneration methods and research prospects. *Fuel* **2024**, *365*, 131184. [CrossRef]
5. Ma, S.; Zhao, X.; Li, Y.; Zhang, T.; Yuan, F.; Niu, X.; Zhu, Y. Effect of W on the acidity and redox performance of the $Cu_{0.02}Fe_{0.2}W_aTiO_x$ (a = 0.01, 0.02, 0.03) catalysts for NH_3-SCR of NO. *Appl. Catal. B Environ.* **2019**, *248*, 226–238. [CrossRef]
6. Binh Ngo, A.; Huyen Vuong, T.; Atia, H.; Weiß, J.; Rabeah, J.; Armbruster, U.; Brückner, A. Role of V and W Sites in $V_2O_5-WO_3/TiO_2$ Catalysts and Effect of Formaldehyde during NH_3-SCR of NO_x. *Chemcatchem* **2022**, *14*, e202200175. [CrossRef]
7. Han, L.; Cai, S.; Gao, M.; Hasegawa, J.-Y.; Wang, P.; Zhang, J.; Shi, L.; Zhang, D. Selective Catalytic Reduction of NO_x with NH_3 by Using Novel Catalysts: State of the Art and Future Prospects. *Chem. Rev.* **2019**, *119*, 10916–10976. [CrossRef] [PubMed]
8. Shi, Z.; Peng, Q.; E, J.; Xie, B.; Wei, J.; Yin, R.; Fu, G. Mechanism, performance and modification methods for NH_3-SCR catalysts: A review. *Fuel* **2023**, *331*, 125885. [CrossRef]
9. Zhao, S.L.; Peng, J.L.; Ge, R.Q.; Yang, K.B.; Wu, S.Y.; Qian, Y.X.; Xu, T.L.; Gao, J.J.; Chen, Y.J.; Sun, Z.Q. Poisoning and regeneration of commercial V_2O_5-WO_3/TiO_2 selective catalytic reduction (SCR) catalyst in coal-fired power plants. *Process Saf. Environ.* **2022**, *168*, 971–992. [CrossRef]
10. Ju, J.R.; Cui, S.T.; Liu, Z.Y.; Yang, W.; Long, T.; Deng, S. Deactivation mechanisms of spent V-Ti-based SCR catalysts and strategies for resource utilization: A systematic review. *Process Saf. Environ.* **2026**, *215*, 109200. [CrossRef]
11. Yin, Y.; Li, K.; Jiang, S.; Peng, Y.; Zhu, T.; Sun, Y.; Li, J.; Li, X. An efficient plasma regeneration of as-poisoned V_2O_5-based catalyst for simultaneous poison removal and activity enhancement. *Chem. Eng. J.* **2024**, *499*, 156141. [CrossRef]
12. Li, J.X.; Zhang, P.; Chen, L.; Zhang, Y.J.; Qi, L.Q. Regeneration of Selective Catalyst Reduction Catalysts Deactivated by Pb, As, and Alkali Metals. *Acs Omega* **2020**, *5*, 13886–13893. [CrossRef] [PubMed]
13. Xue, Y.D.; Zhang, Y.; Zhang, Y.; Zheng, S.L.; Zhang, Y.; Jin, W. Electrochemical detoxification and recovery of spent SCR catalyst by in-situ generated reactive oxygen species in alkaline media. *Chem. Eng. J.* **2017**, *325*, 544–553. [CrossRef]
14. Niu, T.; Wang, J.; Chu, H.; Qian, C.; Duan, N.; Michael Gadd, G.; Shi, W.; Xin, B. Deep removal of arsenic from regenerated products of spent V_2O_5-WO_3/TiO_2 SCR catalysts and its concurrent activation by bioleaching through a novel mechanism. *Chem. Eng. J.* **2021**, *420*, 127722. [CrossRef]
15. Meng, J.; Tong, Z.H.; Zhang, H.Y.; Luo, S.P.; Yu, Y.Y.; Zhang, A.Z.; Qin, H.F. Unveiling the effect of bidentate ligand enhanced sustainable arsenic removal from spent SCR denitration catalyst. *J. Hazard. Mater.* **2026**, *501*, 140826. [CrossRef] [PubMed]
16. Li, M.; Liu, B.; Wang, X.R.; Yu, X.B.; Zheng, S.L.; Du, H.; Dreisinger, D.; Zhang, Y. A promising approach to recover a spent SCR catalyst: Deactivation by arsenic and alkaline metals and catalyst regeneration. *Chem. Eng. J.* **2018**, *342*, 1–8. [CrossRef]
17. Lu, Q.; Ali, Z.; Tang, H.; Iqbal, T.; Arain, Z.; Cui, M.S.; Liu, D.J.; Li, W.Y.; Yang, Y.P. Regeneration of commercial SCR catalyst deactivated by arsenic poisoning in coal-fired power plants. *Korean J. Chem. Eng.* **2019**, *36*, 1016. [CrossRef]
18. Ren, Q.J.; Zhang, G.D.; Huang, X.S.; Tang, Z.C.; Zhang, J.Y. Revealing the deactivation mechanism of Ca poisoning on V-W-Ti catalysts in cement kilns. *Fuel* **2023**, *351*, 128999. [CrossRef]
19. Li, X.; Li, X.; Yang, R.T.; Mo, J.; Li, J.; Hao, J. The poisoning effects of calcium on V_2O_5-WO_3/TiO_2 catalyst for the SCR reaction: Comparison of different forms of calcium. *Mol. Catal.* **2017**, *434*, 16–24. [CrossRef]
20. Li, X.; Li, X.; Chen, J.; Li, J.; Hao, J. An efficient novel regeneration method for Ca-poisoning V_2O_5-WO_3/TiO_2 catalyst. *Catal. Commun.* **2016**, *87*, 45–48. [CrossRef]
21. Li, X.; Liu, C.; Li, X.; Peng, Y.; Li, J. A neutral and coordination regeneration method of Ca-poisoned V_2O_5-WO_3/TiO_2 SCR catalyst. *Catal. Commun.* **2017**, *100*, 112–116. [CrossRef]
22. Chang, H.; Shi, C.; Li, M.; Zhang, T.; Wang, C.; Jiang, L.; Wang, X. The effect of cations (NH_4^+, Na^+, K^+, and Ca^{2+}) on chemical deactivation of commercial SCR catalyst by bromides. *Chin. J. Catal.* **2018**, *39*, 710–717. [CrossRef]
23. Zhang, D.; Wang, C.; Liu, Q.; Liu, Z.; Lei, T.; Wang, B. The combined effects of alkaline-earth metal, SO_2 and CO_2 on the selective catalytic reduction of NO by NH_3 over V_2O_5-WO_3/TiO_2 catalyst. *Environ. Technol. Innov.* **2019**, *14*, 100331. [CrossRef]
24. Lisi, L.; Cimino, S. Poisoning of SCR Catalysts by Alkali and Alkaline Earth Metals. *Catalysts* **2020**, *10*, 1475. [CrossRef]
25. Guo, Y.; Xu, X.; Gao, H.; Zheng, Y.; Luo, L.; Zhu, T. Ca-Poisoning Effect on V_2O_5-WO_3/TiO_2 and V_2O_5-WO_3-CeO_2/TiO_2 Catalysts with Different Vanadium Loading. *Catalysts* **2021**, *11*, 445. [CrossRef]

26. Wang, F.; Wu, X.; Han, Y.; Lv, Y.; Guo, J.; Li, X.; Zhang, Y. Boosting NH_3-SCR Performance and Resistance to K and Ca Poisoning of NbCe/TiNTs Catalyst. *Energ. Fuel* **2025**, *39*, 16387–16398. [CrossRef]
27. Zheng, Y.; Guo, Y.; Wang, J.; Luo, L.; Zhu, T. Ca Doping Effect on the Competition of NH_3–SCR and NH_3 Oxidation Reactions over Vanadium-Based Catalysts. *J. Phys. Chem. C* **2021**, *125*, 6128–6136. [CrossRef]
28. Li, J.Y.; Tang, X.L.; Gao, F.Y.; Yi, H.H.; Zhao, S.Z. Studies on the calcium poisoning and regeneration of commercial De-NO SCR catalyst. *Chem. Pap.* **2017**, *71*, 1921–1928. [CrossRef]
29. Lee, D.-W.; Ahn, Y.; Cho, D.-W.; Basak, B.; Jeon, B.-H.; Choi, J. Evaluation of pyrite/sodium hypochlorite for activating purification of arsenic from fractured-bedrock groundwater. *Environ. Pollut.* **2023**, *317*, 120681. [CrossRef] [PubMed]
30. Wang, C.Z.; Yang, S.J.; Chang, H.Z.; Peng, Y.; Li, J.H. Dispersion of tungsten oxide on SCR performance of $V2O_5$-WO_3/TiO_2: Acidity, surface species and catalytic activity. *Chem. Eng. J.* **2013**, *225*, 520–527. [CrossRef]
31. Hanaor, D.A.H.; Sorrell, C.C. Review of the anatase to rutile phase transformation. *J. Mater. Sci.* **2011**, *46*, 855–874. [CrossRef]
32. Sifontes, A.B.; Cañizales, E.; Toro-Mendoza, J.; Avila, E.; Hernández, P.; Delgado, B.A.; Gutiérrez, G.B.; Diaz, Y.; Cruz-Barrios, E. Obtaining Highly Crystalline Barium Sulphate Nanoparticles via Chemical Precipitation and Quenching in Absence of Polymer Stabilizers. *J. Nanomater.* **2015**, *2015*, 510376. [CrossRef]
33. Xu, T.; Wu, X.; Liu, X.; Cao, L.; Lin, Q.; Weng, D. Effect of barium sulfate modification on the SO_2 tolerance of V_2O_5/TiO_2 catalyst for NH_3-SCR reaction. *J. Environ. Sci.* **2017**, *57*, 110–117. [CrossRef] [PubMed]
34. Viltres, H.; Odio, O.F.; Lartundo-Rojas, L.; Reguera, E. Degradation study of arsenic oxides under XPS measurements. *Appl. Surf. Sci.* **2020**, *511*, 145606. [CrossRef]
35. Lu, Q.; Pei, X.-Q.; Wu, Y.-W.; Xu, M.-X.; Liu, D.-J.; Zhao, L. Deactivation Mechanism of the Commercial V_2O_5–MoO_3/TiO_2 Selective Catalytic Reduction Catalyst by Arsenic Poisoning in Coal-Fired Power Plants. *Energy Fuels* **2020**, *34*, 4865–4873. [CrossRef]
36. Choi, I.H.; Moon, G.; Lee, J.Y.; Jyothi, R.K. Alkali fusion using sodium carbonate for extraction of vanadium and tungsten for the preparation of synthetic sodium titanate from spent SCR catalyst. *Sci. Rep.* **2019**, *9*, 12316. [CrossRef] [PubMed]
37. Tang, X.; Wu, P.; Wang, Y.; Liu, Y. Recent advances in heavy metal poisoning mechanism and regeneration methods of selective catalytic reduction (SCR) denitration catalyst. *Fuel* **2024**, *355*, 129429. [CrossRef]
38. Jones, F.; Jones, P.; Ogden, M.I.; Richmond, W.R.; Rohl, A.L.; Saunders, M. The interaction of EDTA with barium sulfate. *J. Colloid. Interf. Sci.* **2007**, *316*, 553–561. [CrossRef] [PubMed]
39. Hodgson, S.N.B.; Shen, X.; Sale, F.R. Preparation of alkaline earth carbonates and oxides by the EDTA-gel process. *J. Mater. Sci.* **2000**, *35*, 5275–5282. [CrossRef]
40. Murtaza, M.; Rasm, M.Y.; Alarifi, S.A.; Kamal, M.S.; Mahmoud, M.; Al-Ajmi, M. An Efficient Single Step Approach for Barium Sulfate ($BaSO_4$) Scale Removal at High Temperature. *Arab. J. Sci. Eng.* **2023**, *48*, 16879–16888. [CrossRef]
41. Zhang, M.; Zhang, B.; Li, X.H.; Yin, Z.L.; Guo, X.Y. Synthesis and surface properties of submicron barium sulfate particles. *Appl. Surf. Sci.* **2011**, *258*, 24–29. [CrossRef]
42. Dunn, K.; Yen, T.F. Dissolution of barium sulfate scale deposits by chelating agents. *Environ. Sci. Technol.* **1999**, *33*, 2821–2824. [CrossRef]
43. Xu, L.; Niu, S.; Wang, D.; Lu, C.; Zhang, Q.; Zhang, K.; Li, J. Selective catalytic reduction of NO_x with NH_3 over titanium modified $Fe_xMg_yO_z$ catalysts: Performance and characterization. *J. Ind. Eng. Chem.* **2018**, *63*, 391–404. [CrossRef]
44. Chen, C.M.; Cao, Y.; Liu, S.T.; Chen, J.M.; Jia, W.B. Review on the latest developments in modified vanadium-titanium-based SCR catalysts. *Chin. J. Catal.* **2018**, *39*, 1347–1365. [CrossRef]
45. Bulushev, D.A.; Kiwi-Minsker, L.; Rainone, F.; Renken, A. Characterization of surface vanadia forms on V/Ti-oxide catalyst via temperature-programmed reduction in hydrogen and spectroscopic methods. *J. Catal.* **2002**, *205*, 115–122. [CrossRef]
46. Zhang, H.D.; Kong, M.; Cai, Z.L.; Liu, Q.C.; Zeng, J.S.; Duan, M.H.; Yang, J.; Ren, S.; Li, J.L. Comparative Studies of Effects of Vapor- and Liquid-Phase As_2O_3 on Catalytic Behaviors of V_2O_5-WO_3/TiO_2 Catalysts for NH_3-SCR. *Acs Omega* **2020**, *5*, 24195–24203. [CrossRef] [PubMed]
47. Hu, W.S.; Gao, X.; Deng, Y.W.; Qu, R.Y.; Zheng, C.H.; Zhu, X.B.; Cen, K.F. Deactivation mechanism of arsenic and resistance effect of SO_4^{2-} on commercial catalysts for selective catalytic reduction of NO_x with NH_3. *Chem. Eng. J.* **2016**, *293*, 118–128. [CrossRef]
48. Wang, H.M. Acid-mediated reconstruction of $NiFeO_x$ for boosting NH_3-SCR performance: Optimizing redox-acid sites via sulfuric acid functionalization. *Sep. Purif. Technol.* **2026**, *388*, 136762. [CrossRef]

49. Yang, N.-Z.; Guo, R.-T.; Tian, Y.; Pan, W.-G.; Chen, Q.-L.; Wang, Q.-S.; Lu, C.-Z.; Wang, S.-X. The enhanced performance of ceria by HF treatment for selective catalytic reduction of NO with NH_3. *Fuel* **2016**, *179*, 305–311. [CrossRef]
50. Roy, S.; Viswanath, B.; Hegde, M.S.; Madras, G. Low-Temperature Selective Catalytic Reduction of NO with NH_3 over $Ti_{0.9}M_{0.1}O_{2-\delta}$ (M = Cr, Mn, Fe, Co, Cu). *J. Phys. Chem. C* **2008**, *112*, 6002–6012. [CrossRef]

Disclaimer/Publisher's Note: The statements, opinions and data contained in all publications are solely those of the individual author(s) and contributor(s) and not of MDPI and/or the editor(s). MDPI and/or the editor(s) disclaim responsibility for any injury to people or property resulting from any ideas, methods, instructions or products referred to in the content.